Hindawi
Journal of Advanced Transportation
Volume 2023, Article ID 8072495, 16 pages
https://doi.org/10.1155/2023/8072495

Research Article

Driving Risk Field and Control Strategies for Autonomous Vehicles at a Signalized Intersection

Hui Xu [1,2] **and Jianping Wu** [1]

[1]*Department of Civil Engineering, Tsinghua University, Beijing 100084, China*
[2]*CCDI Exploration & Design Consultant Co., Ltd., No. 276 Dongping Road, Suzhou 215125, Jiangsu, China*

Correspondence should be addressed to Hui Xu; xu.hui4@ccdi.com.cn

Received 29 April 2023; Revised 12 June 2023; Accepted 28 July 2023; Published 28 August 2023

Academic Editor: J. Ingda Wu

Driving pattern has been increasingly researched to improve driving safety and develop autonomous vehicles. Oriented towards the complex infrastructures at signalized intersections, this research digs into the risk sources brought by different kinds of road elements, including road lane markings, road curbs, median separators, signal timing, and neighboring vehicles around the ego car. Referring to vehicle speed both in the longitudinal and latitudinal dimensions, risk scope and distribution are quantified with the vehicle position of a torus with a Gaussian cross-section. Then, the risk is summed over all the road elements across all the points involved by the ego car, the level of which should be controlled within the threshold value when the ego vehicle explores to minimize trip delay. Thus, autonomous driving strategies are developed with respect to vehicle speed and steering angle. The proposed model is validated with NGSIM data, where a signalized intersection on Peachtree Street is selected and vehicles moving in different directions are analyzed. It is found that the proposed model manages to control vehicles with risk at the accepted level and to enhance the speed level as well as reduce acceleration fluctuations. This research contributes to improving autonomous driving against complex driving conditions for driving safety and efficiency.

1. Introduction

Driving through signalized intersection is a complex task, where drivers are required to pay close attention to many interruptions and obstacles, either from the road infrastructures (e.g., the yellow/white solid/dotted lanes) or from the neighboring vehicles [1, 2]. Ego vehicles observe and immediately respond to these road elements with vehicle state adjustment in both speed and steering angle for safe driving, from which driving patterns can be explored for the development of autonomous driving. With the accumulated literature on signalized intersection safety, driving risk evaluations and controls through signalized intersections are increasingly improved to promote more efficient response strategies.

Driving risks at signalized intersections have long been explored for driving safety and accident reduction. Statistically, there are over 50% injuries and fatalities that occur near the signalized intersections, where driver errors are the leading cause [3]. Based on the k-means cluster analysis and hierarchical Bayesian random intercept models, driver injury severity patterns of intersection-related crashes find that drivers' behavioral adjustment to sophisticated external environmental conditions may compensate for crash loss but to unstable degrees. Motivated by the complex interactions between the driver and the environment, studies have been increasingly accumulated, e.g., for the risk perception of roundabouts [4]. Safety performance functions have been established to predict crash frequencies and reductions with countermeasures on risk exposure. To explore the impact of driving behaviors, negative binomial models are developed to explore the relationships of driving crash frequency with the factors of average annual daily traffic, speed, deceleration, acceleration, right-turn lanes, left-turn signal phase, and red-light camera, where right-turn lanes are negatively correlated to crash frequency, while left-turn

signal phase has a positive association with crash frequency [5]. On the conflict between right-turn vehicles and pedestrian at signalized intersection, male and young pedestrians as well as the ones that have waited for a long time take more risks [6]. At the onset of yellow light at signalized intersections, drivers may behave with low-risk or high-risk, where the former are only slightly disturbed by phone calls and more prone to stop when close to the stop line [7].

Referring to the theory of field and potential, driving risk field (DRF) has been introduced into the evaluation of vehicle operation risk. DRF is validated to be correlated to the driver's perceived risk and manual driving behaviors in terms of steering angle and speed [8]. Based on the framework of artificial field theory to treat all the obstacles to the subject vehicle as a finite scalar risk field, a better basis to access driving safety is established, which considers the uncertainty over future ambient traffic state and the magnitude of crash consequences with the target vehicle in some position at a certain speed [9]. At signalized intersections, the effect of yellow light on driving risk field has been carefully addressed [10]. Consequently, the vehicle trajectory planning model is developed to address driver's dilemma at yellow light. With the advancement of connected automated vehicles, we may employ the DRF method based on accurate real-time data to help adjust vehicle states by considering the inhomogeneous coefficients of vehicle geometry and direction [11]. Simulation-based conflict analyses have also been established for signalized intersection, where comparison is implemented between the simulated and field-measured conflicts for safety assessment [12].

The response strategies to the risks at intersections have also been extensively studied. For minimal fatalities and property loss in crashes, infrastructure-cooperative intersection accident warning system has been developed to predict vehicle state evolution based on dynamic Bayesian networks for temporal stochastic process, with the input of the factors of traffic light state, vehicle position, speed, acceleration/deceleration, and heading, as well as driver's behavioral variable. The model is validated to warn the driver when potentially dangerous driving behaviors are detected [13]. For driving safety and efficiency as well as fuel saving, deep reinforcement learning is employed to train the connected and automated vehicles, which can accurately communicate with the surrounding vehicles and signal light, from the scratch for cooperative vehicular operation at signalized intersections on the simulation platform [14]. A generalized critical turning point-based hierarchical decision-making and planning method is developed in various shapes of intersections with median strips and multiple road lines, which is calibrated with real-driving dataset [15]. Furthermore, to examine whether the advanced driving warning system has increased risky behaviors, the hierarchical logistic regression model and the random forest algorithm are developed to find that, when the driver is distracted, speeding, or driving in high-density traffic, the likelihood of hard-braking behaviors can be significantly increased [16]. The motion-planning method with intelligent driver model for autonomous vehicles has also been developed to drive through unsignalized intersections, where future vehicle states are predicted with appropriate clearance and time of collision [17].

When looking onto the complex driving conditions on the urban roads, we are motivated to examine the combined effects of all kinds of road elements, including road lane lines, median barriers, road signs, access, intersection geometry, and signal control, in addition to the moving elements such as neighboring vehicles [18, 19]. Despite the accumulated research in driving risk, still there are few works attempting to reveal the vehicle risk at signalized intersection, a typical motorized environment [20]. The response strategies to the established risks from the abovementioned road elements are also called for to flexibly address all kinds of obstacles to the ego vehicle [21, 22], that is, the vehicle should follow the pipe defined by road furniture or road markings and to keep distance from the neighboring vehicles on the same or different lanes, under the objective of minimal trip delay with driving risk at the reasonable level [23]. Thus, a comprehensive analysis framework is established to decode the effect of different types of road elements on driving risks and lay a foundation for the development of autonomous driving for safety and efficiency.

The contributions of the research are three-fold. First, all the basic elements at a typical signalized intersection are analyzed with respect to the possible risks they bring about. These elements include the static ones, including multiple road-lane lines, road curbs, median separators, turning curves, and signal timing. Risk from each element is decoded, which decreases as the ego vehicle moves away from them, with the probability of the ego vehicle at each neighboring point obeying Gaussian distribution. Second, response strategies from the ego vehicle are established to avoid the abovementioned obstacles, where the signal driving strategy is developed to address the dilemma caused by yellow light, and the longitudinal and latitudinal driving strategies are proposed for vehicle state adjustment. Furthermore, the proposed risk quantification method and the obstacle response strategies are validated with the NGSIM data [24], proving its accuracy and efficiency of guiding the vehicle to move downward safely.

The remaining of the research is organized as follows: Section 2 illustrates the risks source of all kinds of road elements at a typical signalized intersection and risk distribution against vehicle state of direction, speed, and steering angle, Section 3 establishes the response strategies of vehicles against different scenarios, considering the operation constraints to the ego vehicle of either road geometry, road markings, signal timing, and neighboring vehicles, Section 4 employs NGSIM data to validate the proposed risk evaluation method and obstacle response strategies, and Section 5 briefly concludes the study with the research plan in future.

2. Road Elements and Potential Risk Field

2.1. Conceptual Framework and Basic Assumptions. Figure 1 shows the layout of typical signalized intersections, including both static and moving road elements. It is observed that the lane lines on the approach change from dotted white to solid white around tens of meters upstream of the stop line. Amber double solid lane lines are employed to separate the vehicles of opposite directions. Signal light controls the movement of straight and left-turning vehicles, while the movement of right-turning vehicles is not controlled. Here, the interruptions from pedestrians and bicyclers are not specifically considered for model simplification. Instead, we focus on the movable elements of neighboring vehicles either on the same or different lanes. The basic assumptions of the research are as follows:

(1) Only vehicles are considered for moving road elements, while pedestrians and bicycles are not considered. Signal control includes green light, amber light, and red light, without flashing light.

(2) Autonomous driving system may accurately observe the dynamics of neighboring vehicles and the design of the road infrastructures against stable communication conditions, based on which driving risks can be accurately calculated to develop vehicle control strategies.

(3) Autonomous driving system explores to minimize travel delay through the signalized intersection with driving risk not higher than the threshold.

Figure 2 gives the basic procedure of implementing the analyses of driving risk field at the signalized intersection. First, the research scope is defines vehicle trajectories, which are extracted for left-turning, straight, and right-turning traffic. Then, the static and moving road elements around the ego vehicle are identified as risk source, the risk distribution of which is quantified in proportion to the distance between the ego vehicle and each road element. In the following, we will dig into the effects of each road element on driving adjustments for driving safety and efficiency.

2.2. Road Elements and Risk Sources

2.2.1. Lane Markings. Lane markings can be categorized into various types, which can be yellow or white and solid or broken. Yellow lines separate traffic in the opposite directions, whereas the broken yellow lines can be crossed if necessary, while solid yellow lines should never be crossed. White lines separate the lanes in the same direction, whereas the broken white lines mean that one may move across it when safe, while the solid white lines require one to stay in the lane. Figure 3 shows the cost of crossing different lane markings. It is observed that, crossing white broken lines brings the least cost, followed by crossing yellow dotted lines, while crossing the white solid lane brings appreciable cost due to the penalty of violating traffic rule and crossing a yellow solid line corresponds to even higher cost [25]. Parameters C_{ws} and C_{ys} are employed to represent the cost of wheel rolling on the solid white lane line and solid yellow lane line, respectively; and parameters C_{wd} and C_{yd} mean the cost of moving onto white dotted and yellow dotted lines.

2.2.2. Median Separator and Road Curb Stone. Vehicle collision with median separator can cause serious damage to both the vehicle and separator, the cost of which is demonstrated in Figure 4 against different kinds of road median separators. Hitting the green division or metal division may cause the vehicle's serious deformation and wheel damage, similar to the collision with the curb stone in Figure 5.

Note in the literature, one may introduce the definition of road boundary potential filed, which extends to infinity as the ego vehicle approaches the road curb or median separator [26]. Actually, the cost of colliding with the road boundary can be quantified with the average cost, instead of being set infinite. That is closely related to vehicle class and speed. The conflict severity can be given by the following:

$$M = m \times \left(1.566 \times 10^{-14} \times v^{6.687} + 0.3345\right), \quad (1)$$

where M represents the expected conflict severity and v represents the vehicle speed. That is, the larger the vehicle's actual mass and the higher the vehicle's speed, the higher the expected conflict severity. The cost of colliding with road boundary is given by the following:

$$C_b = M \times E_b, \quad (2)$$

where parameter E_b represents the unit cost of colliding with road boundary per equivalent vehicle weight.

2.2.3. Road Signs. Road signs guide vehicles to operate on the proper path at suitable state, including vehicle weight, height, and speed. For example, if one vehicle runs at the speed higher than the limit, it may receive a speeding ticket or fail to be controlled in case there is emergency. Therefore, vehicles may only operate not higher than the speed limit and always keep the rule. The cost of breaking the traffic rules by road signs can be given by the following:

$$C_s = \sum_n E_{sn} \times d_{sn}, \quad (3)$$

where n refers to the nth signs faced by the ego car, E_{sn} refers to the unit cost from violating the traffic rule given by sign n, and d_{sn} means the degree level of violating traffic rules. For example, if the speed limit is set at 50 km, 10% higher than the limit is not punished, while speeding between 10% and 20% is punished to a lesser degree than that between 20% and 30%, etc.

2.2.4. Signal Light. The potential field of signal light starts ahead of the stop line. The first road segment involving driving cost is the dilemma zone, where vehicles have difficulty in both moving through and stopping ahead of the stop line [27]. If the vehicle chooses to stop ahead of the stop line at the yellow light, the distance that the vehicle drives through can be given by the following:

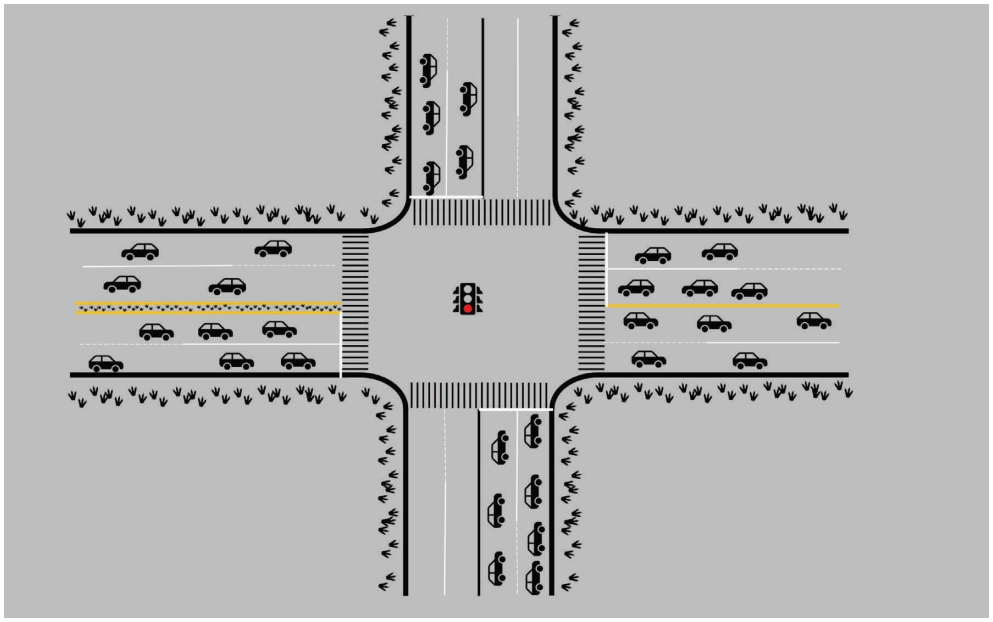

Figure 1: Illustration of moving and static road elements at a signalized intersection.

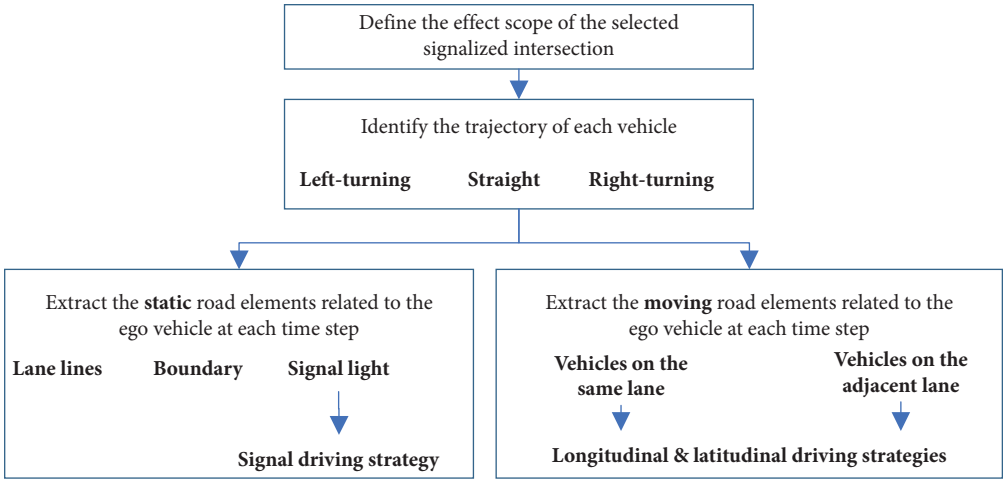

Figure 2: Framework of recognizing the risks of different road elements.

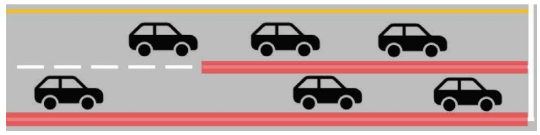

Figure 3: Risks of crossing the road line markings.

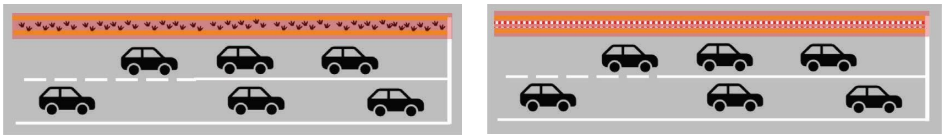

(a) (b)

Figure 4: Risks of colliding with road median separators. (a) Median separator of green division. (b) Median separator of metal isolation barrier.

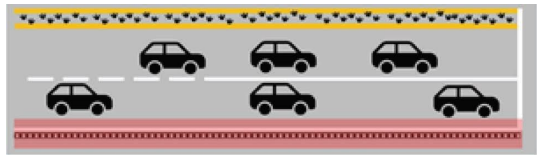

Figure 5: Risks of colliding with the curb stone.

$$X_s = v_0 \times \tau_1 + \frac{{v_0}^2}{2d}, \tag{4}$$

where v_0 is the initial vehicle speed, τ_1 represents the reaction time to brake, and d means the maximum deceleration speed. Instead, if the vehicle chooses to move through the intersection, the maximum distance that the vehicle can drive through is given by the following:

$$X_c = v_0 \times \tau_2 + \frac{1}{2}a(\tau - \delta_2)^2 - (W + L), \tag{5}$$

where τ_2 is the reaction time to decide to drive through, a is the maximum acceleration, τ is the yellow time interval, W is the intersection width, and L is the vehicle length. The dilemma emerges when $X_s > X_c$, as shown in Figure 6. In contrast, if $X_s \le X_c$, the driver may choose to stop or to move downstream of the stop line.

In the case of $X_s > X_c$, when amber light is on, if the ego vehicle is more than X_s from the stop line, the ego vehicle should choose to stop. Thus, the cost of moving past the stop line at the second that yellow light turns on (i.e., C_{syr}) is set sufficiently large. Otherwise, if the distance of it from the stop line is less than X_s, the ego vehicle may adjust the driving state to seize the chance to move through the stop line. Thus, the risk from yellow light is given by the following:

$$C_{\text{syr}} = \begin{cases} C_M, & \text{if } X_d > X_s \,\&\, X_s > X_c, \\ C_x, & \text{if } X_d \le X_s \,\&\, X_s > X_c, \\ C_M, & \text{if } X_d > X_C \,\&\, X_s \le X_c, \\ 0, & \text{if } X_d \le X_C \,\&\, X_s \le X_c, \end{cases} \tag{6}$$

where X_d represents the distance of the target vehicle from the stop line. Parameters C_M and C_X represent randomly large driving cost, and adjustable driving risk, respectively.

2.2.5. Moving Road Elements and Potential Field. Here, we focus on the vehicular dynamics for simplification because the description of pedestrian and bike crossings can make the model much more complex. Referring to the Yukawa potential [28] proposed in physics, short-range force is employed here to describe the interactions among the surrounding vehicles, risks from which pose direct effect on the driving strategy of the ego vehicle.

Figure 7 shows the vehicles that directly interact with the ego car (i.e., the green one). In addition to the leading and following vehicles of the ego car on the same lane, the vehicles most close to the ego vehicle on the adjacent lanes are also included, that is, the vehicles not behind and the vehicle immediately behind the ego car on the adjacent lane are considered as the related moving elements. Note the moving elements may change from time to time as vehicles change lanes. Thus, the related moving elements should be selected each time interval.

Note the collision cost between the ego and the neighboring vehicles is also dependent on the vehicle speed, which is given by the following:

$$C_v = M_e \times M_n \times e_v, \tag{7}$$

where the parameters M_e and M_n refer to the equivalent mass of the ego vehicle and its neighboring vehicles, considering their speed, and parameter e_v refers to the unit cost of vehicle collision per equivalent vehicle weight.

2.3. Risk Field

2.3.1. Risk Distribution of Road Elements. With vehicle longitudinal and lateral speed, if the driver fails to control the vehicle in time, it may run onto road obstacles or markings and be involved with different driving costs. Thus, the risk source of road elements can be delivered to the ego vehicle when their distance is shorter than the following:

$$\begin{aligned} d_{x0} &= \left(v_x \times T + \frac{{v_x}^2}{2d} \right) + \varepsilon, \\ d_{y0} &= \left(v_y \times T + \frac{{v_y}^2}{2d} \right) + \varepsilon, \end{aligned} \tag{8}$$

where d_{x0} and d_{y0} are the distances traveled by the ego vehicle after it recognizes the driving cost and manages to brake to stop in the lateral and longitudinal direction, respectively, parameters v_x and v_y are the vehicle speeds in the lateral and longitudinal directions, respectively, T represents driver's reaction time, and ε is the stop distance between the ego vehicle and road elements. Parameters v_x and v_y are given by the following:

$$\begin{aligned} v_x &= v \times \cos\delta, \\ v_y &= v \times \sin\delta, \end{aligned} \tag{9}$$

where parameter δ is the vehicle heading angle, which is initiated with the road angle and updated using the following:

$$\delta = \delta_0 + k \times \Delta\delta, \tag{10}$$

where δ_0 refers to the vehicle heading angle in the previous step, parameter k represents the coefficient of vehicle angle adjustment, and $\Delta\delta$ means the difference from vehicle heading to road direction. The longer the distance between

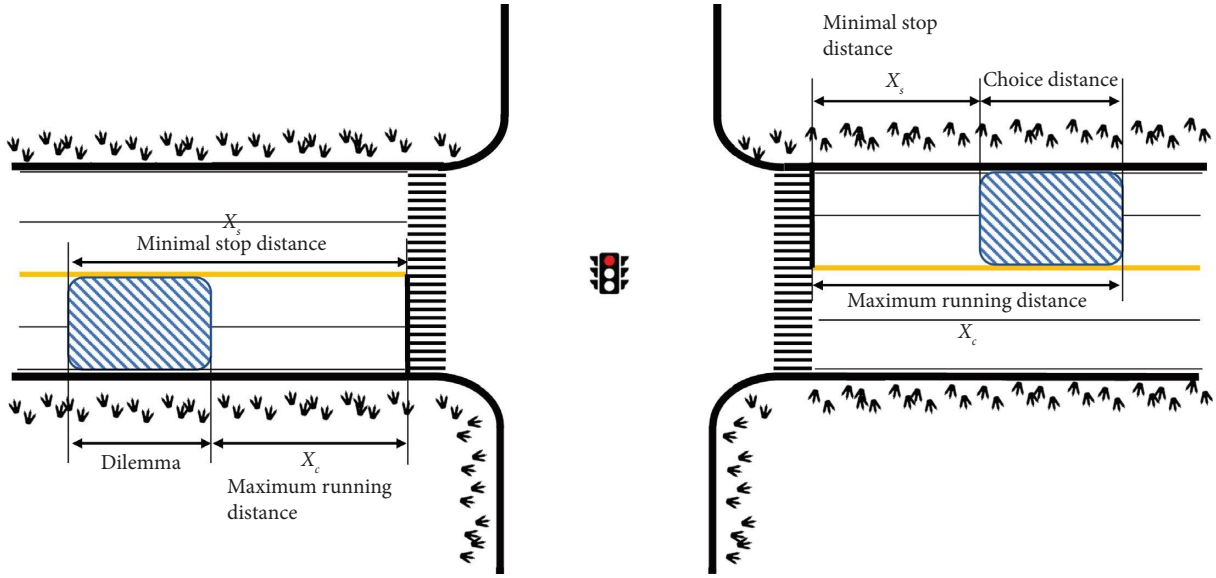

Figure 6: Illustration of dilemma zone and the choice zone.

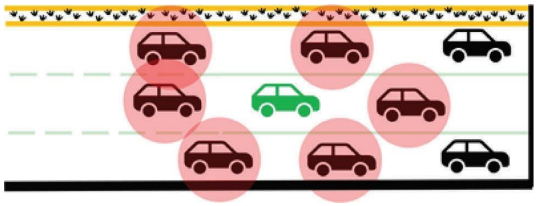

Figure 7: Cost incurred by the surrounding vehicles based on short-range force.

the ego vehicle and the road obstacle, the smaller the cost that can be added to the vehicle. Thus, driving risk from different road elements to the ego vehicle is given by the following:

$$C_x = \begin{cases} C_n \times \dfrac{d_{x0} - d_x}{d_{x0}}, & \text{if } d_{x0} > 0, d_{x0} \geq d_x, \\ 0, & \text{otherwise,} \end{cases}$$
$$C_y = \begin{cases} C_n \times \dfrac{d_{y0} - d_y}{d_{y0}}, & \text{if } d_{y0} > 0, d_{y0} \geq d_y, \\ 0, & \text{otherwise,} \end{cases} \tag{11}$$

where parameter C_n refers to the cost from the n^{th} road elements in the previous section, d_x and d_y are the actual distance between the edge of the road cost and the ego vehicle in the lateral and longitudinal directions, respectively. The final risk incurred by the ego vehicle is given by the following:

$$C = \min \{C_x, C_y\}. \tag{12}$$

2.3.2. Probability Distribution of Vehicle Position. This research takes the method of a torus with Gaussian cross-section to calculate the probability of the ego vehicle moving to the position (x, y), which is then multiplied with the risks caused by different road elements. That is, the total risk for the ego vehicle can be given by the following:

$$R = \sum_{(x,y)} z_{xy} \times C, \tag{13}$$

where z_{xy} represents the probability of the ego vehicle moving to point (x, y), given by the following [29]:

$$z(x, y) = a \times \exp\left[-\frac{(d_{xy} - R)^2}{2\sigma^2}\right], \tag{14}$$

which is a torus with a Gaussian cross-section. Parameter a is the height of the Gaussian, d_{xy} is the distance between the risk point and the ego car point, R is the vehicle turning radius, and σ is the Gaussian width.

Gaussian height a is given by

$$a(s) = p(s - v \times T)^2, \tag{15}$$

where p is the slope of Gaussian curve, s is the curve length between the risk point and the car position, and v is the vehicle speed. Curve length is given by

$$s = R \times |\theta|, \tag{16}$$

where R represents the circle radius of the ego vehicle, and θ is the angle intersected by the lines connecting the circle center (x_c, y_c) and the ego vehicle position (x, y) or connecting the circle center and the risk position (x', y'). Circle radius R is given by the following:

$$R = \frac{L}{\tan\varphi},$$
$$\theta = \arccos\left(\frac{(x - x_c)(x' - x_c) + (y - y_c)(y' - y_c)}{\sqrt{(x - x_c)^2 + (y - y_c)^2} \times \sqrt{(x' - x_c)^2 + (y' - y_c)^2}}\right), \tag{17}$$

where φ is the vehicle steering angle to be updated with the new vehicle heading angle, given by the following:

$$\varphi = \varphi_0 + dt \times \left(\frac{v}{L}\right) \times \tan\delta, \tag{18}$$

where φ_0 refers to the vehicle heading angle in the previous step and dt means the length of the control step. The distance between the vehicle and the risk point in equation (14) is given by the following:

$$d_{xy} = \sqrt{(x' - x)^2 + (y' - y)^2}. \tag{19}$$

Gaussian width σ is given by the following:

$$\sigma_i = (q + k_i|\delta|)s + c, \tag{20}$$

where i represents the inner and outer side of the vehicle, i.e., $i = 1$ for the inner side and $i = 2$ for the outer side, parameter q is Gaussian width slope, k_i is the slope of the variability brought by vehicle steering angle of the inner and outer side of $i = 1$ or $i = 2$, and parameter c is the Gaussian width at the vehicle location, which is related to the car width (w) and takes the value of $w/4$ to make $\pm 2\sigma$ account for 95% risk.

3. Response Strategies against Risk Potential Field

3.1. Vehicle Control Framework. Figure 8 shows the logic framework for vehicle response strategies against the potential field from various road elements. For the trajectory of the ego vehicle, the involved traffic elements, static or moving, are outlined with their potential risks. Then, the critical problem of evaluating the driving strategy at signalized intersection is to identify the phase switch from green light to yellow light, at which the driving risk increases greatly if the vehicle cannot move through the remaining distance from the stop line. Thus, the signal driving strategy is developed first to examine the cost exerted by the start of yellow light. In the following, the longitudinal driving strategy is developed to guide the vehicles to operate on the same lane or change onto the adjacent lanes. Then, the latitudinal driving strategy takes the decisions from signal and longitudinal driving strategies to return the vehicle speed and steering angle.

Figure 9 shows the relationship of signal, longitudinal, and latitudinal driving strategies. First, the signal driving strategy explores to take stronger acceleration or smaller headway. Then, the longitudinal driving strategy explores vehicle intention of car-following, lane-changing, and accelerating based on the current vehicle state. The requirements from signal and longitudinal driving strategies are incorporated into latitudinal driving strategy against the objective of minimal driving delay and proper risk level via adjustment in vehicle speed and steering angle.

3.2. Driver's Algorithm. Figure 10 illustrates the signal's driving strategy. When yellow light turns on, if the ego vehicle is following some car, it may explore for smaller headway if possible. If the ego vehicle is the leading car, it may take stronger acceleration than in the general case as long as the speed is not higher than the speed limit to seize the yellow light.

Figure 11 shows the longitudinal strategy to control vehicle states in different situations. Referring to road conditions, the driving state of the ego vehicle is extracted, to which the adoption of signal driving strategy is judged first. If there is no additional driving strategy, we come to the point to judge if there is leading vehicle of the ego car. If the ego car is leading on the current lane, it will explore for the possibility of acceleration; if the ego car is following another car, it will search for a faster lane, which means that the leading vehicle on the adjacent lane runs at a higher speed. If there is a faster lane and the lane-change gap is available, the ego car will come to the latitudinal driving algorithm; otherwise, the ego vehicle continues to follow the leading car on the current lane.

Taking the decisions from signal driving strategy and longitudinal driving strategy, latitudinal driving strategy is developed together with speed adjustment. That is, driving strategies from signal and longitudinal state just add general guide to the vehicles, instead of accurate directions on vehicle state changes. When it comes to latitudinal driving strategies, vehicle speed and steering angle are optimized against the specific driving risk field.

Figure 12 shows the framework of latitudinal driving strategy. When the perceived driving risk is lower than the threshold and vehicle speed is lower than the speed limit, the algorithm explores to enhance vehicle speed within the speed limit, where parameter Δ_{vn} means the increase in the rate of vehicle speed in the n^{th} situation; if the signal driving strategy is adopted to require more stronger acceleration, Δ_{vn} can be set at a larger value as indicated with $n = 1$; if not, Δ_{vn} takes a small value with $n = 2$. If the perceived driving risk is higher than the threshold, while the speed limit is not reached, we may explore the necessity of deceleration, i.e., whether steering itself may reduce driving risk to the expected level. This is achieved by performing grid search, an optimization algorithm that is computationally efficient to return a satisfying solution, especially to the sophisticated

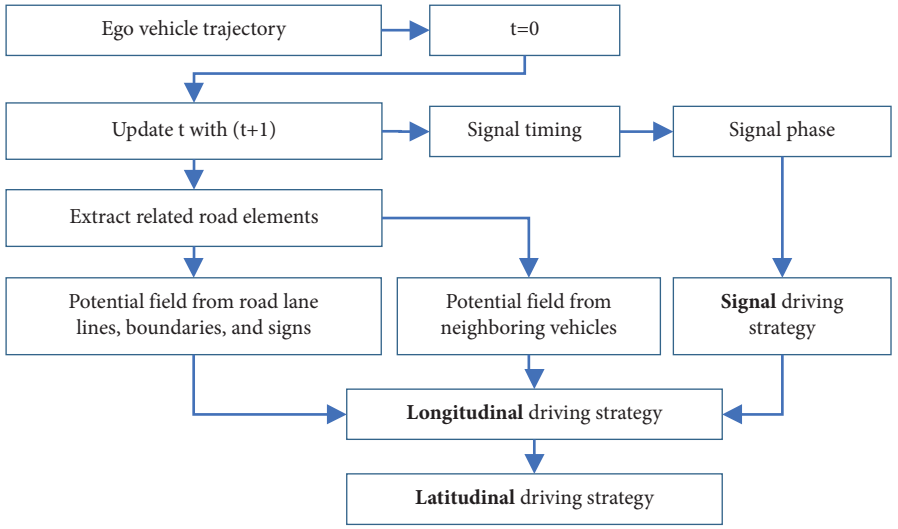

Figure 8: Procedures of signal, longitudinal, and latitudinal driving strategies.

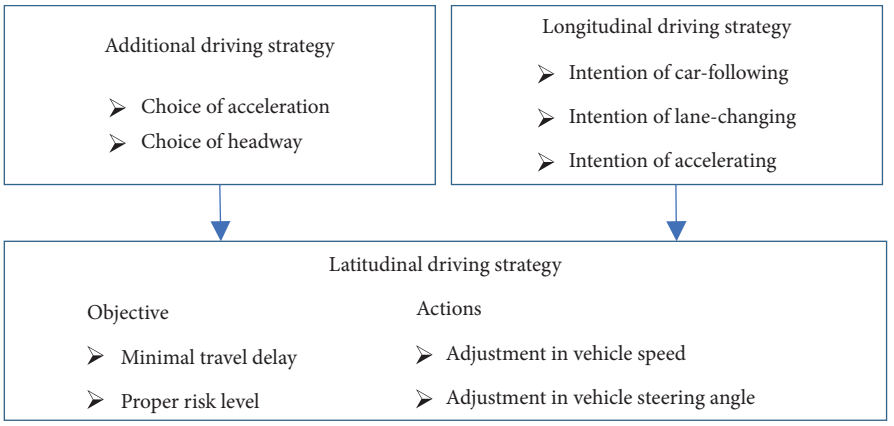

Figure 9: The relationship of signal, longitudinal, and latitudinal driving strategies.

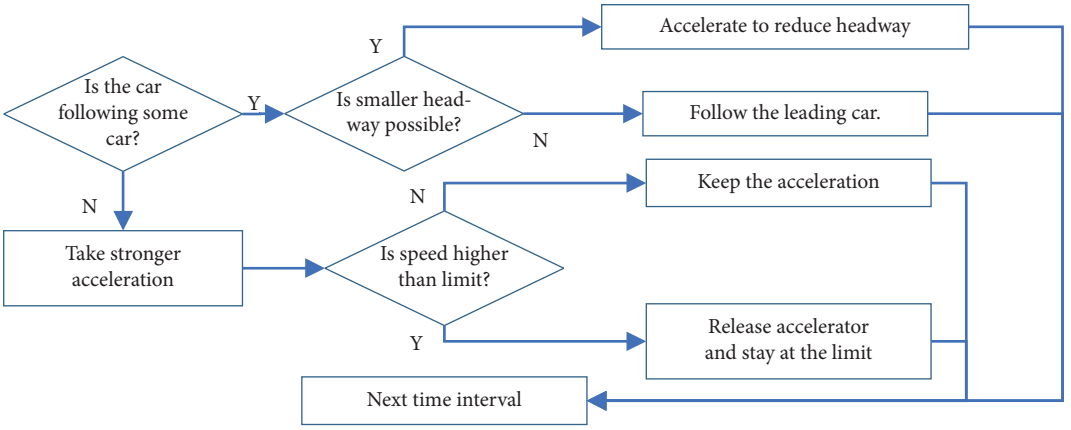

Figure 10: The algorithm of additional driving strategy.

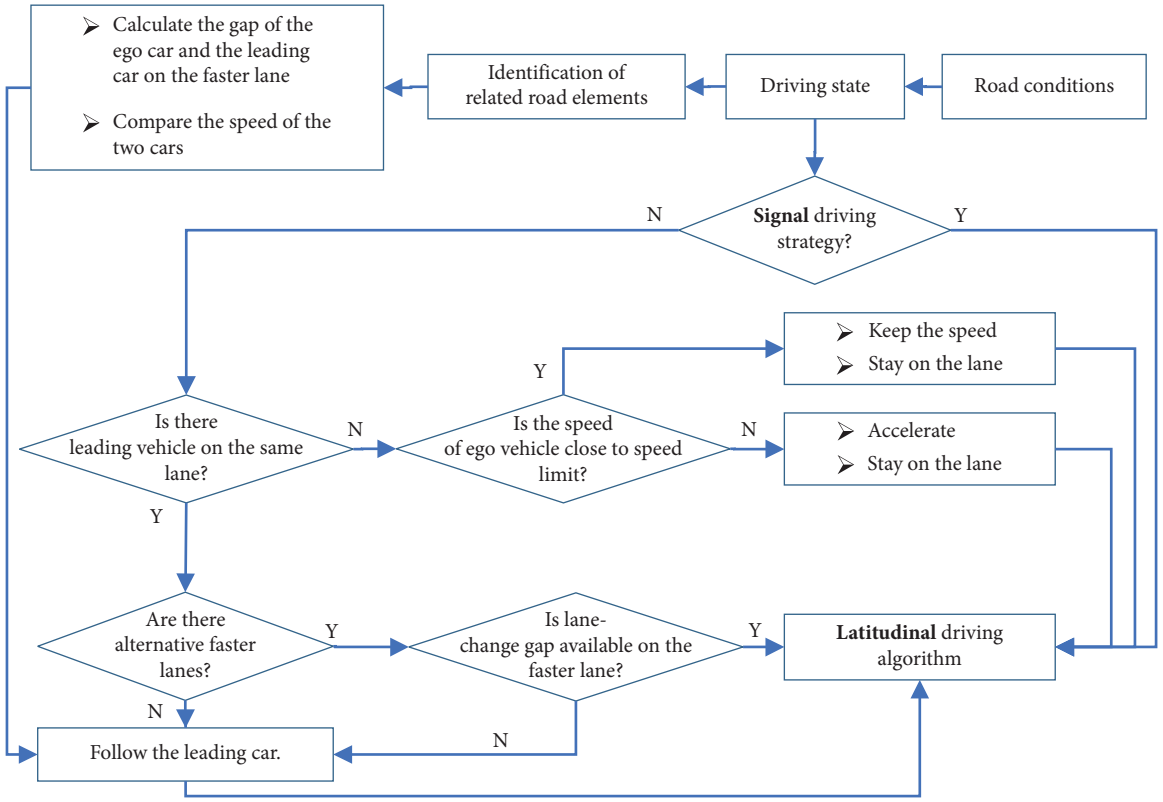

Figure 11: The algorithm of longitudinal driving strategy.

problems with noise or nonsmoothness. Grid search first generates uniform grid inputs for the objective function to identify the areas of the search space that deserve more attention. Then, each variable is enumerated in turn, from which the best performing point is identified and reported.

Thus, the optimal steering angle at the vehicle's current speed is explored and returned. If the optimal θ manages to reduce the risk lower than the threshold and deceleration is not necessary, vehicle steering angle is updated for risk equal to threshold, and vehicle speed increases within the limit. Otherwise, if deceleration is necessary, vehicle speed decreases in proportion to the gap between risk threshold and risk at current, and steering angle takes the value to reduce risk to the risk threshold. Furthermore, if vehicle risk is higher the threshold and speed is higher than the limit, vehicle decelerates proportional to the gap both in risk and speed.

4. Case Study

4.1. Scenario Design. NGSIM database is adopted on Peachtree Street (Atlanta) for detailed car trajectory, which was collected between 12:45 p.m. and 13:00 p.m. on November 8, 2006. Vehicle trajectories are recorded, with real-time speed, acceleration, x and y position, the following/leading car, time headway, spacing headway, and time stamp with the interval of one-tenth second. Figure 13 shows the signalized intersection selected for calibrating and validating the proposed model. Here, many static road elements can be observed, including the yellow solid lane line, white solid lane line, white dotted lane line, curb stone, pedestrian crossing, and signal light. The road markings can be obtained with the CAD file, and the signal timings are collected via CSV files.

Taking the northbound approach for example, solid yellow line is set in the road center to separate the vehicles in the opposite direction. The first lane on the northbound approach is exclusively for left turning, which is marked with the central solid yellow line and the right-side white solid lane. The second lane is exclusively for straight vehicles, which is separated with dotted lane line from the third lane that serves both straight and right-turning vehicles. The first lane connects to the left-turning curve, which starts immediately downstream of the pedestrian crossing, while the third lane connects to right-turning curve, which is parallel to the curb stone. Figure 14 shows the trajectory of vehicles on each lane of the selected intersection, where the coordinates of road elements are identified. Figure 15 gives the signal timing control of the four phases, the cycle of which is 95 s with all-red time being 1.9 s. Note the green light for left turning on the 10^{th} street starts at the 36^{th} time interval.

Figure 16 shows the procedure to preprocess vehicle data and to extract vehicle trajectory. Data preprocessing is implemented with respect to the vehicle speed change, vehicle displacement, and vehicle steering angle. The range of reasonable steering range is calculated with the maximum steering angle of 20 degrees, and the ratio of steering wheel and wheel turning being 50. With the processed data, data are selected with vehicle position on y axis no more than 400 feet, which fully covers the selected intersection. Vehicles are

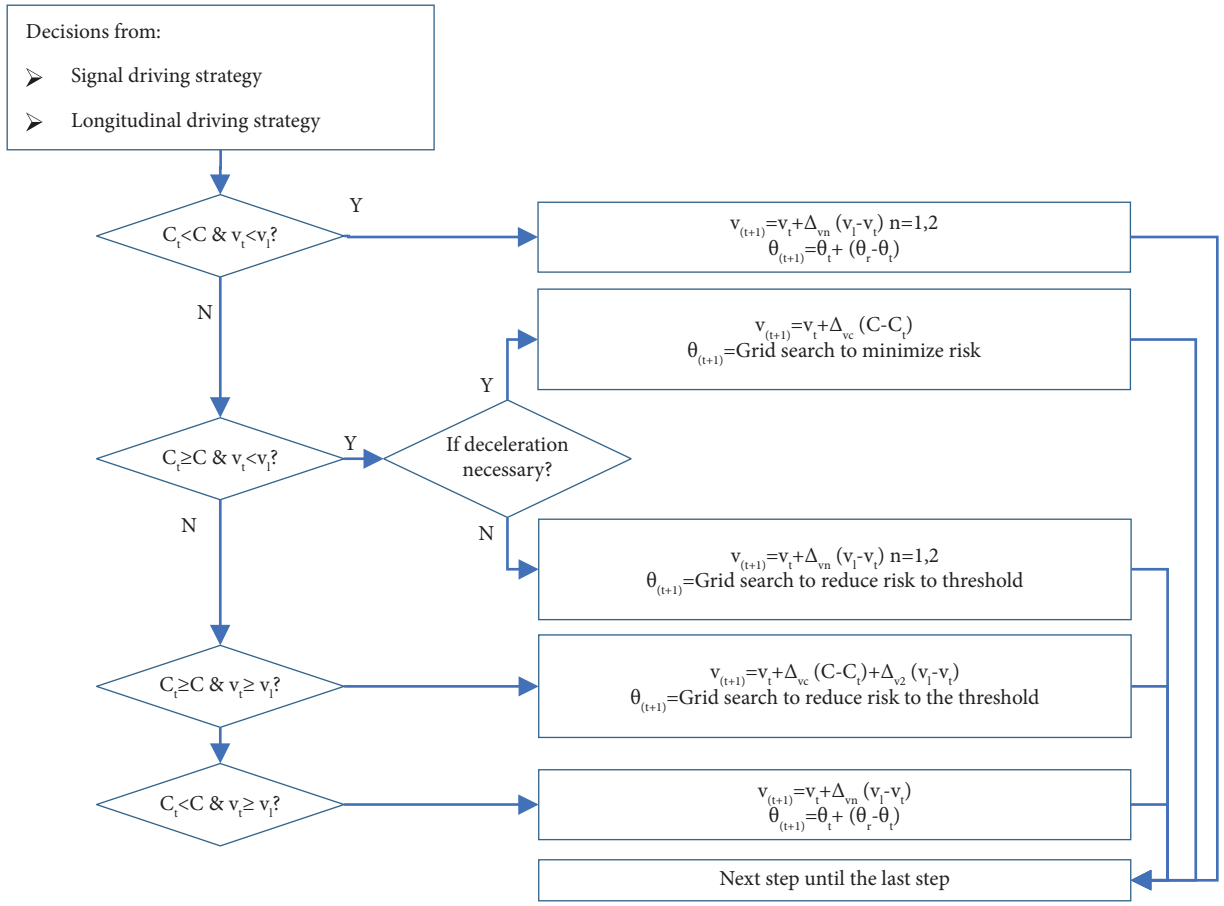

Figure 12: The algorithm of latitudinal driving strategy.

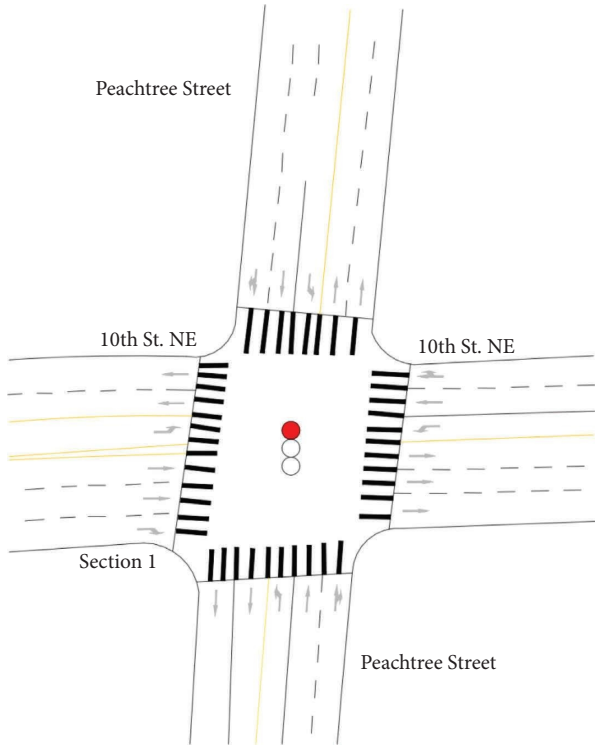

Figure 13: The selected signalized intersection on Peachtree Street in NGSIM database.

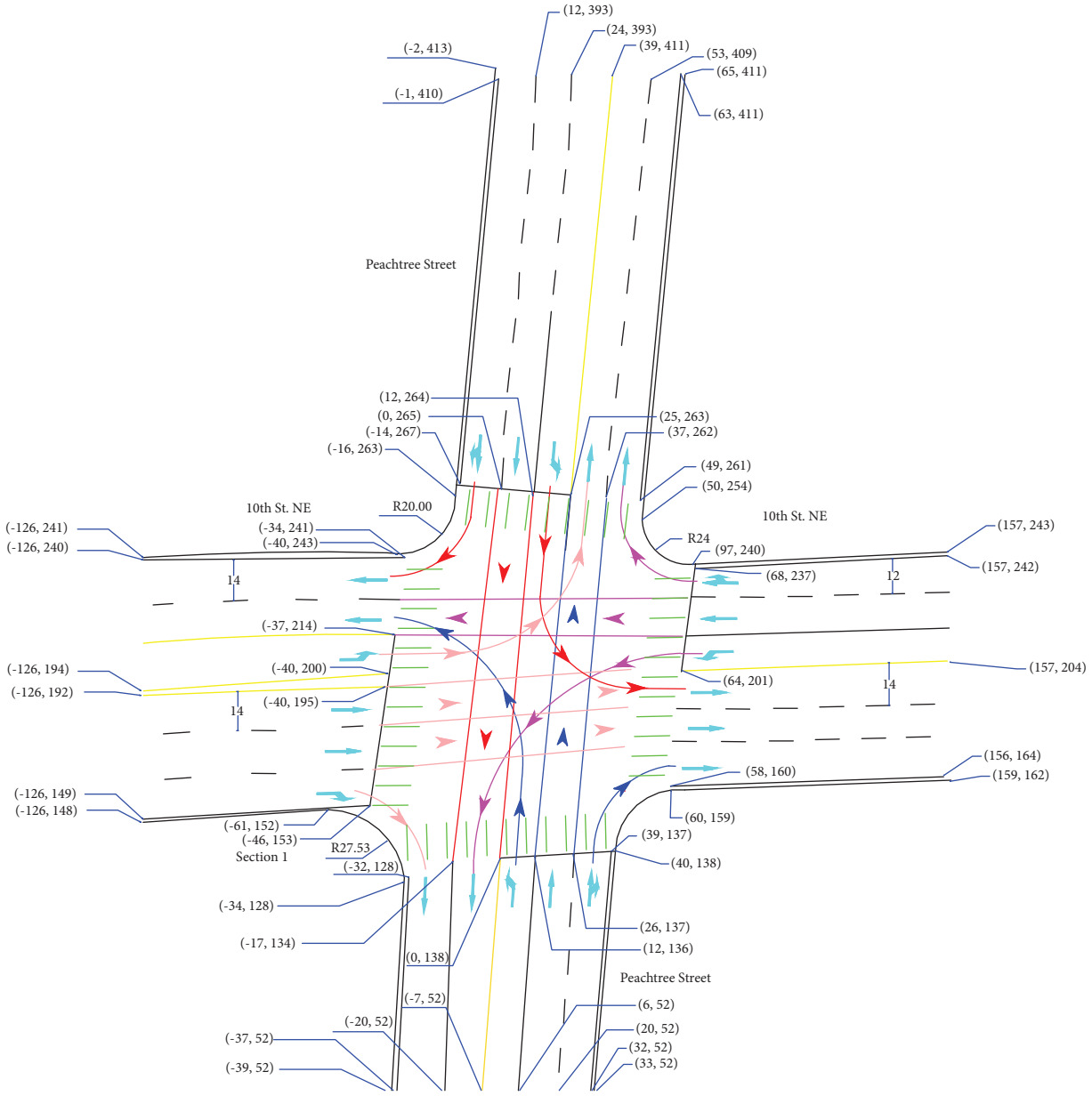

Figure 14: Vehicle trajectory at the selected signalized intersection.

identified with the attributes of vehicle ID, total frames count, vehicle length, vehicle width, vehicle origin, and vehicle destination. The frame count of each vehicle is calculated with the last frame ID minus the first frame ID.

Table 1 summarizes the parameters of risk modeling of different road elements, with the parameter values of the Gaussian torus borrowed from the literature [23]. Table 2 gives the parameter values of driver's algorithm, which are obtained with grid search by establishing support vector machine for the regression of these model parameters for maximal likelihood. In this step, 70% of the selected data are employed for model training, while the remaining 30% are employed to test the proposed model.

4.2. Results and Discussions. This section analyzes the results of the proposed driving strategy against the developed driving risk field from the comprehensive road elements at the signalized intersection. Figure 17 shows the curves of vehicle latitudinal position, longitudinal position, speed, and acceleration against time of the typical vehicles in the test dataset. It is observed that the model can generally replicate vehicle trajectories, where the simulated vehicle's longitudinal and latitudinal positions from the proposed model are close to the real-data. Note that the proposed driving strategy can be returned to the vehicle within 0.01 second, sufficiently efficient to guide vehicle driving.

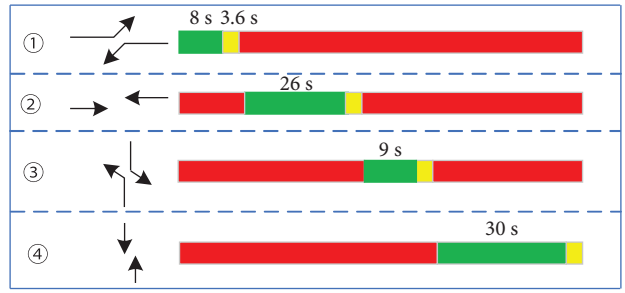

Figure 15: Signal timing at the selected intersection with phase 2 starting at the 36th time interval.

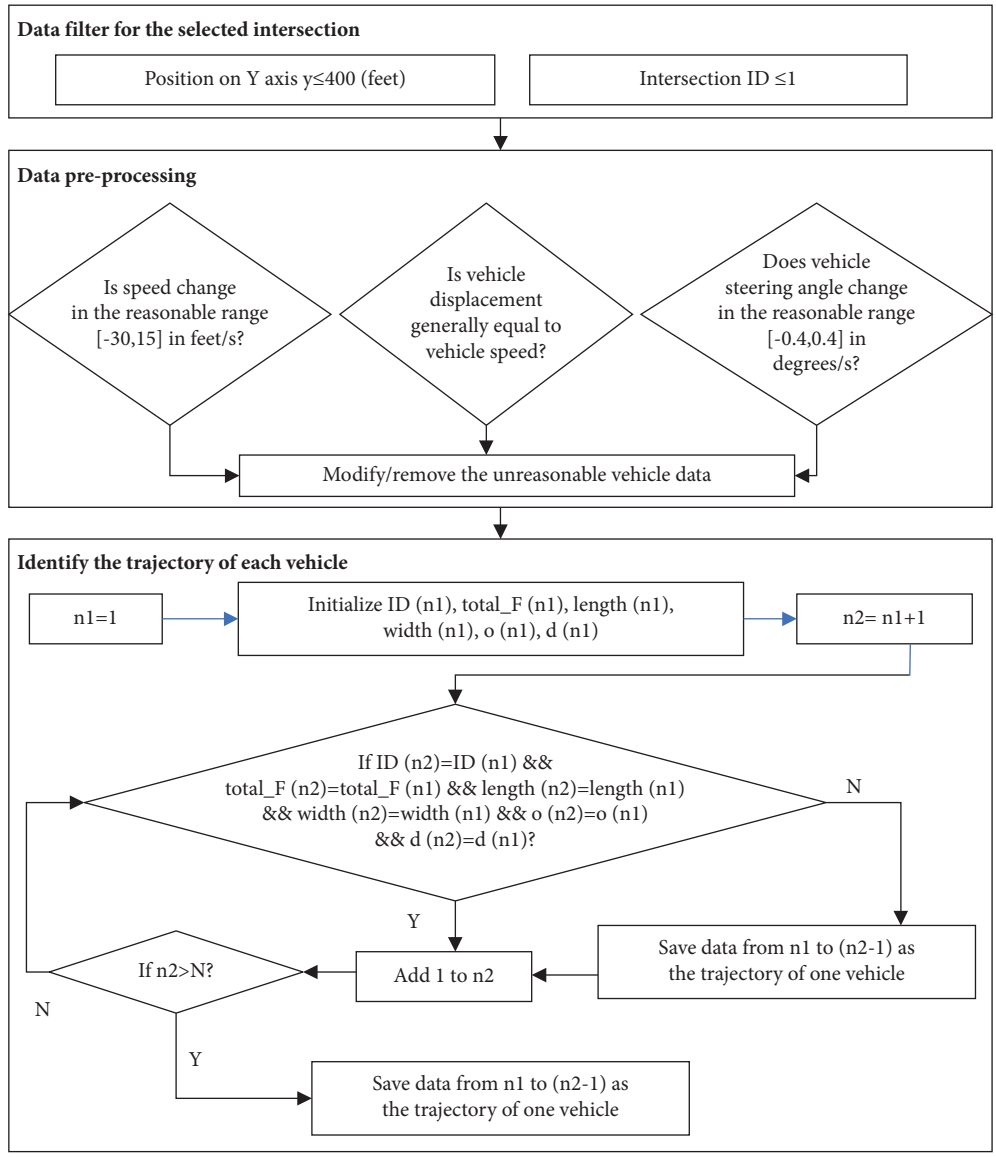

Figure 16: The framework for extracting vehicle trajectory and data preprocessing.

Figure 18 summarizes the benefit of the proposed model with respect to vehicle speed and acceleration, where the proposed autonomous driving strategies manage to improve the vehicle speed and reduce acceleration fluctuations. It is observed that the straight and right-turn vehicular movements are better improved compared to left-turning movements. This can be explained with more constraints of road elements for straight and right-turn movements, e.g., more neighboring vehicles for straight vehicles and road curb for right-turn vehicles. In contrast, left-turn vehicles are

Table 1: Parameters of risk field model.

No.	Notation	Explanation	Value
1	C_{ws}	Cost of wheel rolling on the solid white lane line	1
2	C_{ys}	Cost of wheel rolling on the solid yellow lane line	3
3	C_{wd}	Cost of wheel rolling on the dotted white lane line	0.3
4	m	Vehicle weight of motorcycle, automobile, truck/bus	0.3 t, 1.5 t, 10 t
5	E_b	Unit cost of colliding with road boundary	1
6	E_{sn}	Unit cost of speeding over the limit of 50 mile/h	1
7	d_{sn}	Level of violating speed limit: 0–10%, 10%–20%	0, 1
8	τ_1	Reaction time to brake to stop	1.5 s
9	τ_2	Reaction time to decide to drive through	1.5 s
10	d	Maximum deceleration	5 m/s^{-2}
11	a	Maximum vehicle acceleration	3 m/s^{-2}
12	W	Intersection width of Peachtree Street and 10th street	110 feet, 90 feet
13	L	Vehicle length	As in NGSIM
14	C_{syr}	Cost of moving past the stop line before green light	1000
15	e_v	Unit collision cost with neighboring vehicle	2
16	T	Driver reaction time	1.5 s
17	ε	Safe distance between the vehicle and road elements	(i) 100 m for road sign (ii) 0.3 m for road lines (iii) 2 m for signal light
18	A	A randomly large constant	10000
19	p	Slope of Gaussian curve	0.0064
20	q	Gaussian width slope	0.001
21	k_i	Variability slope by vehicle steering angle	(i) $k_1 = 0$ for inner turning (ii) $k_2 = 1.38$ for outer

Table 2: Parameters of driver model.

No.	Notation	Explanation	Value
1	C	Risk threshold	1.96
2	v_1	Speed limit	50 mile/h
3	Δ_{vn}	Acceleration slope by the gap from speed limit	(i) 0.31 for strong acceleration ($n = 1$) (ii) 0.14 otherwise ($n = 2$)
4	Δ_{vc}	Acceleration slope to reduce the gap from speed limit	0.07

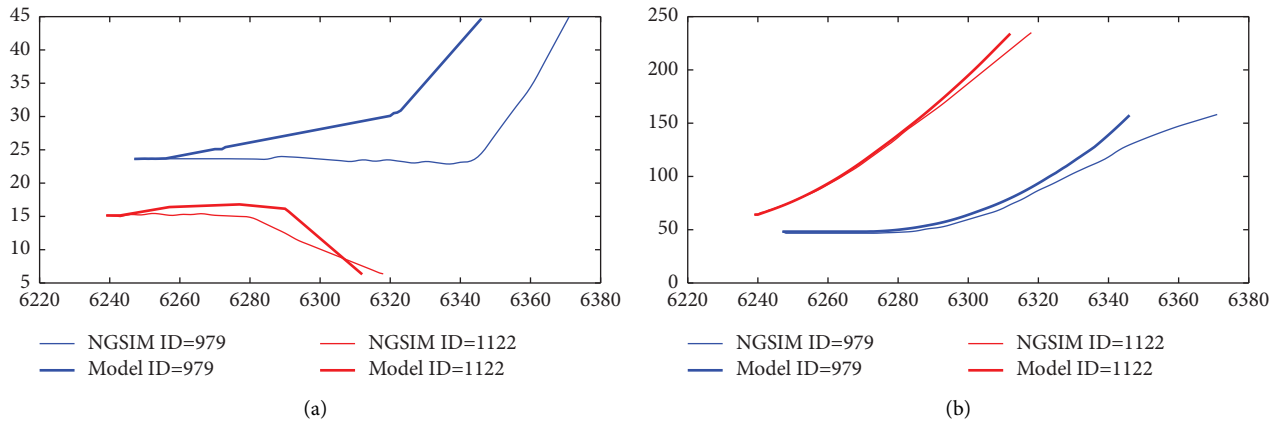

(a) (b)

Figure 17: Continued.

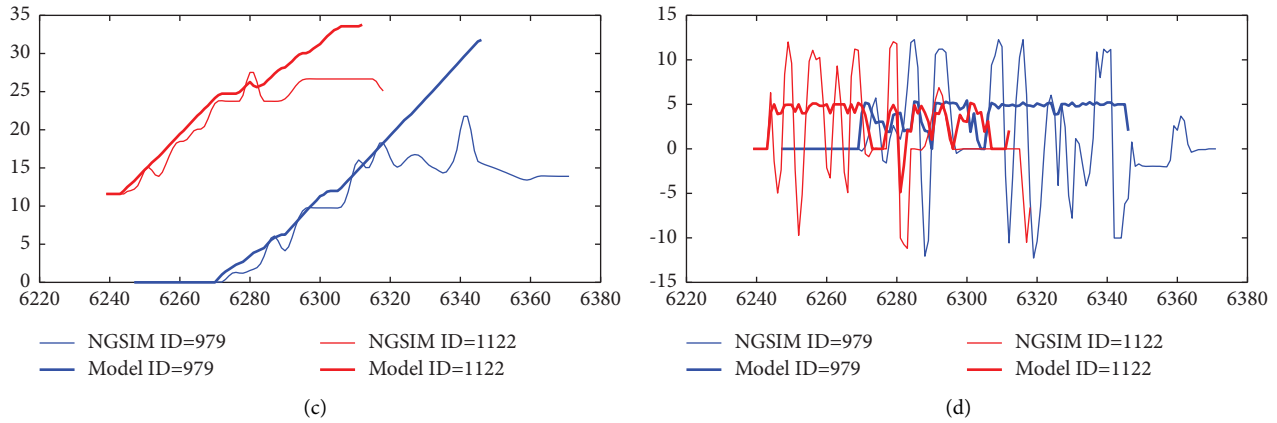

Figure 17: Vehicle states from the proposed model in comparison to that in the test dataset. (a) Vehicle latitudinal position. (b) Vehicle longitudinal position. (c) Vehicle speed. (d) Vehicle acceleration.

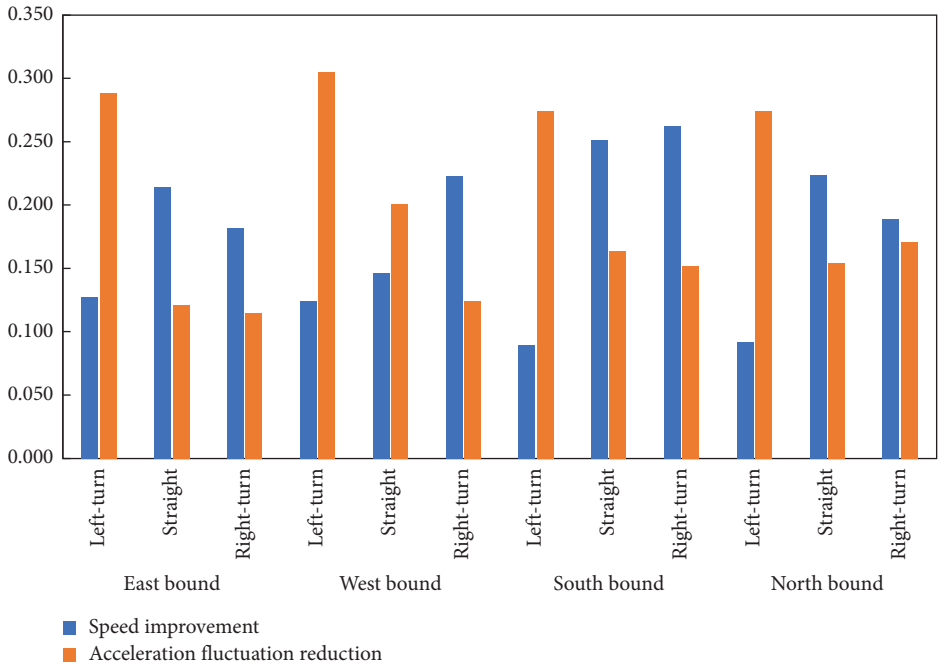

Figure 18: Benefits of the proposed autonomous driving strategies based on risk field.

open to more freedom to adjust operation trajectory. Thus, there is smaller space for the autonomous driving strategies to make use of higher speed of left-turn vehicles, where acceleration fluctuation is the most reduced with persistent and reliable control.

5. Conclusions

Driving safety is basic to every driver, for whom driving efficiency is also pursued. In this process, drivers must respond to various interruptions and follow the constraints posed by all kinds of road elements, either movable or nonmovable. With the increasing research on driving risk evaluation and driving assistance system, the comprehensive model of driving risk field has been developed to reflect the effect of various road elements on vehicle operation, instead of being limited to one or a few elements. This research extends the theory of driving risk field at the signalized intersection, where driving risks from all kinds of road lane lines, neighboring vehicles, and signal timings are analyzed systematically. The cost of each kind of road lane lines is analyzed based on the possible cost from touching or crossing the road element. Specifically, the cost of passing the solid lane line is evaluated with the penalty of violating the traffic rule, while the cost of colliding with the road curb is evaluated with the cost to vehicle damage and to road furniture repair. The cost of signal timing is carefully addressed since the start of the yellow light, when the vehicle may have difficulty in deciding to move across the stop line to stop upstream of it. Moreover, the cost from the

neighboring vehicles is calculated with reference to the short-distance force theory, where the nearby vehicles are recognized to be following or leading the ego vehicle on the same lane or on the right/left-side lane.

In the following, driving strategy against various driving risks is developed. First, the control framework is developed to examine vehicle's distance to different road elements and the state of signal light. Then, the longitudinal and latitudinal driving strategies are developed to respond to the constraints on vehicles' downward movement and to the constraints on vehicles' adjustment within or beyond one lane. Model calibration and validation is implemented based on NGSIM data of an urban street, where a typical four-legged signalized intersection is selected. After preprocessing of the selected data, the parameters are calibrated for the proposed model. The accuracy of the proposed model is evaluated with RMSE for the vehicles on all the legs of the selected intersection. It is found that, the accuracy of the proposed model is lower on the intersection approach compared to that on the exit, with RMSE being 14.2%, 19.3%, and 11.6% for vehicle speed, longitudinal position, and latitudinal position on the approach, compared to 16.9%, 19.7%, and 23.1% on the exit. This can be explained with more driving freedom on the intersection exit.

Limitations of the research are three-fold. First, driving behavior and driver's characteristics are not specifically considered in the proposed model, which may affect drivers' perception and evaluation of road risks to cause the difference in the driving strategy adoptions. Second, the influence of pedestrians and bicyclers is not addressed for model simplicity, which may radically change the driving mechanism. For example, when the driver senses the possibility of colliding with a man or a rider, he may change driving trajectory much earlier and fully secure the gap between the planned trajectory and the predicted conflict points. Third, the proposed model should be further validated in extensive road conditions, validating its performance against different driving environments.

Future research may extend the research to incorporate the impact of driver's characteristics into the evaluation of and response to the driving risk field, to better reflect driving dynamics along the selected road. Another fruitful avenue is to integrate driving assistance system into the driving risk field to guide vehicles to better adapt to the changing road environment for safety enhancement, especially against immediate interruptions.

Data Availability

NGSIM data are employed in the research, please visit https://catalog.data.gov/dataset/next-generation-simulation-ngsim-vehicle-trajectories-and-supporting-data.

Conflicts of Interest

The authors declare that they have no conflicts of interest.

Authors' Contributions

Hui Xu was responsible for the conceptualization, methodology, survey, software, validation, and analyses, and Jianping Wu was responsible for draft preparation and project administration. Both authors have read and agreed to the submitted version of the manuscript.

Acknowledgments

This work was supported by the Science and Technology Project of Jiangsu Province construction system (Grant no. 2022ZD10004).

References

[1] Y. Liu and U. Ozguner, "Human driver model and driver decision making for intersection driving," in *2007 IEEE Intelligent Vehicles Symposium*, pp. 642–647, IEEE, Istanbul, Turkey, June 2007.

[2] P. Chen and J. Zhou, "Effects of the built environment on automobile-involved pedestrian crash frequency and risk," *Journal of Transport and Health*, vol. 3, no. 4, pp. 448–456, 2016.

[3] Z. Li, C. Chen, Y. Ci et al., "Examining driver injury severity in intersection-related crashes using cluster analysis and hierarchical Bayesian models," *Accident Analysis and Prevention*, vol. 120, pp. 139–151, 2018.

[4] L. Salvatore, D. Natalia, and P. Giulia, "Multiple Correspondence Analysis (MCA) for the evaluation of risk perception of roundabouts for young people," *European Transport\Trasporti Europei*, vol. 72, no. 4, 2019.

[5] A. Mohammadnazar, A. L. Patwary, N. Moradloo, R. Arvin, and A. J. Khattak, "Incorporating driving volatility measures in safety performance functions: improving safety at signalized intersections," *Accident Analysis and Prevention*, vol. 178, Article ID 106872, 2022.

[6] A. Kumar, M. Paul, and I. Ghosh, "Analysis of pedestrian conflict with right-turning vehicles at signalized intersections in India. Journal of Transportation Engineering," *Part A: Systems*, vol. 145, no. 6, 2019.

[7] J. Li, B. Jiang, C. Dong, J. Wang, and X. Zhang, "Analysis of driver decisions at the onset of yellow at signalized intersections," *Journal of Advanced Transportation*, vol. 2020, Article ID 2023093, 12 pages, 2020.

[8] S. Kolekar, B. Petermeijer, E. Boer, J. de Winter, and D. Abbink, "A risk field-based metric correlates with driver's perceived risk in manual and automated driving: a test-track study," *Transportation Research Part C: Emerging Technologies*, vol. 133, Article ID 103428, 2021.

[9] F. A. Mullakkal-Babu, M. Wang, X. He, B. van Arem, and R. Happee, "Probabilistic field approach for motorway driving risk assessment," *Transportation Research Part C: Emerging Technologies*, vol. 118, Article ID 102716, 2020.

[10] J. Hua, G. Lu, and H. X. Liu, "Modeling and simulation of approaching behaviors to signalized intersections based on risk quantification," *Transportation Research Part C: Emerging Technologies*, vol. 142, Article ID 103773, 2022.

[11] Y. Tian, H. Pei, J. Yang, J. Hu, Y. Zhang, and X. Pei, "An improved model of driving risk field for connected and automated vehicles," in *In 2021 IEEE International Intelligent*

Transportation Systems Conference (ITSC), pp. 285–291, IEEE, Indianapolis, IN, USA, September 2021.

[12] Y. Guo, M. Essa, T. Sayed, M. M. Haque, and S. Washington, "A comparison between simulated and field-measured conflicts for safety assessment of signalized intersections in Australia," *Transportation Research Part C: Emerging Technologies*, vol. 101, pp. 96–110, 2019.

[13] Y. Fu, C. Li, T. H. Luan, Y. Zhang, and G. Mao, "Infrastructure-cooperative algorithm for effective intersection collision avoidance," *Transportation Research Part C: Emerging Technologies*, vol. 89, pp. 188–204, 2018.

[14] M. Zhou, Y. Yu, and X. Qu, "Development of an efficient driving strategy for connected and automated vehicles at signalized intersections: a reinforcement learning approach," *IEEE Transactions on Intelligent Transportation Systems*, vol. 21, no. 1, pp. 433–443, 2020.

[15] K. Shu, H. Yu, X. Chen et al., "Autonomous driving at intersections: a behavior-oriented critical-turning-point approach for decision making," *IEEE/ASME Transactions on Mechatronics*, vol. 27, no. 1, pp. 234–244, 2022.

[16] B. Yu, S. Bao, Y. Chen, and D. J. LeBlanc, "Effects of an integrated collision warning system on risk compensation behavior: an examination under naturalistic driving conditions," *Accident Analysis and Prevention*, vol. 163, Article ID 106450, 2021.

[17] Y. Jeong and K. Yi, "Target vehicle motion prediction-based motion planning framework for autonomous driving in uncontrolled intersections," *IEEE Transactions on Intelligent Transportation Systems*, vol. 22, no. 1, pp. 168–177, 2021.

[18] N. Lyu, L. Xie, C. Wu, Q. Fu, and C. Deng, "Driver's cognitive workload and driving performance under traffic sign information exposure in complex environments: a case study of the highways in China," *International Journal of Environmental Research and Public Health*, vol. 14, no. 2, p. 203, 2017.

[19] S. Q. Xie, N. Dong, S. C. Wong, H. Huang, and P. Xu, "Bayesian approach to model pedestrian crashes at signalized intersections with measurement errors in exposure," *Accident Analysis and Prevention*, vol. 121, pp. 285–294, 2018.

[20] A. Sheykhfard and F. Haghighi, "Driver distraction by digital billboards? Structural equation modeling based on naturalistic driving study data: a case study of Iran," *Journal of Safety Research*, vol. 72, pp. 1–8, 2020.

[21] Y. Rasekhipour, A. Khajepour, S. K. Chen, and B. Litkouhi, "A potential field-based model predictive path-planning controller for autonomous road vehicles," *IEEE Transactions on Intelligent Transportation Systems*, vol. 18, no. 5, pp. 1255–1267, 2017.

[22] B. Lu, G. Li, H. Yu et al., "Adaptive potential field-based path planning for complex autonomous driving scenarios," *IEEE Access*, vol. 8, pp. 225294–225305, 2020.

[23] S. Kolekar, J. de Winter, and D. Abbink, "Human-like driving behaviour emerges from a risk-based driver model," *Nature Communications*, vol. 11, no. 1, p. 4850, 2020.

[24] Y. Zhou and Y. Chen, "Learning to drive in the NGSIM simulator using proximal policy optimization," *Journal of Advanced Transportation*, vol. 2023, Article ID 4127486, 12 pages, 2023.

[25] J. Wang, J. Wu, and Y. Li, "The driving safety field based on driver–vehicle–road interactions," *IEEE Transactions on Intelligent Transportation Systems*, vol. 16, no. 4, pp. 2203–2214, 2015.

[26] L. Li, J. Gan, Z. Yi, X. Qu, and B. Ran, "Risk perception and the warning strategy based on safety potential field theory," *Accident Analysis and Prevention*, vol. 148, Article ID 105805, 2020.

[27] D. Gazis, R. Herman, and A. Maradudin, "The problem of the amber signal light in traffic flow," *Operations Research*, vol. 8, no. 1, pp. 112–132, 1960.

[28] H. Yukawa, "On the interaction of elementary particles. I," *Proceedings of the Physico-Mathematical Society of Japan. 3rd Series*, vol. 17, pp. 48–57, 1935.

[29] S. Kolekar, J. De Winter, and D. Abbink, "Which parts of the road guide obstacle avoidance? Quantifying the driver's risk field," *Applied Ergonomics*, vol. 89, Article ID 103196, 2020.